GEOFIZIKA VOL. 42 2025

DOI: https://doi.org/10.15233/gfz.2025.42.7
Original scientific paper

Microearthquake identification and seismicity analysis of the M4.7 Feidong earthquake sequence in Anhui

Yu Wang [1], *Shiwen Xie* [2], *Pan Guo* [3] *and Junhao Qu* [1]

[1] Shandong Earthquake Agency, JiNan, China

[2] Anhui Earthquake Agency, Hefei, China

[3] Liaoning Earthquake Agency, Shenyang, China

Received 8 April 2025, in final form 3 July 2025

On September 18, 2024, an M4.7 earthquake struck Feidong County in Hefei, Anhui Province. Located at the complex junction of the Tanlu fault zone, this event exhibited a clear foreshock–mainshock–aftershock evolution, attracting widespread attention. To investigate the aftershock activity and seismogenic structure of this earthquake sequence, this study employs deep learning methods applied to continuous waveform data from the Anhui seismic network for automatic detection. Coupled with precise earthquake relocation, a comprehensive and high-precision seismic catalog was constructed. The relocation results indicate that the Earthquake sequence are mainly distributed along a linear trend in the NE–SW direction, extending approximately 12 km, with hypocentral depths concentrated between 8 and 13 km. Notably, both the mainshock and most aftershocks occur at a depth of about 10.5 km. Focal mechanism solutions reveal that the dominant earthquakes in the region exhibit right-lateral strike-slip rupture on steeply dipping faults trending NE, which is highly consistent with the orientation and structural characteristics of the primary Zhuding–Shimenshan fault in the area. In conjunction with observational evidence of fluid intrusion, it is inferred that fluids may have migrated from the southwest into the seismogenic zone through structural pathways such as the Zhuding–Shimenshan fault and accumulated within a depth range of approximately 10 km near the fault. This fluid accumulation likely induced local stress concentration, which may be the primary trigger for the Feidong earthquake sequence.

Keywords: deep learning, double-difference relocation, focal mechanism solution, seismogenic structure

1. Introduction

Based on data provided by the China Earthquake Networks Center (CENC), a magnitude 4.7 earthquake occurred at 20:08 on September 18, 2024, in Feidong

County, Anhui Province (31.98° N, 117.60° E) with a hypocentral depth of 12 km and an intensity of VI on the Modified Mercalli scale. The earthquake sequence exhibited clear foreshock–mainshock–aftershock characteristics: three significant foreshocks occurred prior to the mainshock (a M3.5 event on February 24, a M3.1 event on May 12, and a M3.9 event on September 14), while aftershocks of M3.8 and M3.3 were recorded on September 25 and October 1, respectively. As the most significant seismic event recorded by modern instruments in Hefei, this earthquake, occurring approximately 37 km from the city center, generated substantial social impact.

Seismic identification and phase picking form the cornerstone of precise earthquake relocation. Accurate phase arrival times enable the construction of a high-precision earthquake catalog, which is crucial for revealing the evolution of seismic clusters, deciphering triggering mechanisms, and understanding nucleation processes. With the deployment of high-density seismic networks, the volume of monitoring data has grown exponentially, rendering traditional manual processing methods inadequate for modern seismic monitoring needs and driving an urgent demand for efficient, automated detection techniques (Yuan, 2022). Consequently, the automatic detection and relocation of microearthquakes have emerged as a frontier in seismological research. Template matching methods based on waveform similarity (Shelly, 2007; Zhang, 2019) detect events by calculating the cross-correlation coefficient between continuous waveforms and predefined templates, thereby significantly enhancing detection sensitivity compared to manual approaches. However, these methods suffer from high template dependency and intensive computational resource demands, limiting their applicability in real-time processing scenarios (Zhou, 2021). In recent years, deep learning has rapidly advanced seismic phase identification, with Convolutional Neural Network (CNN) models achieving precise P- and S-wave arrival detection and first-motion polarity classification. Notably, PhaseNet—an evolution of the U-Net architecture (Zhu and Beroza, 2019)—has outperformed traditional STA/LTA and AR-Picker techniques in both detection sensitivity and phase picking accuracy, as evidenced by superior F1 scores across numerous monitoring networks worldwide. Moreover, multimodal neural network fusion strategies have further enhanced performance; for instance, a hybrid model combining CNN and RNN, developed by Zhou et al. (2019) and trained on the Wenchuan aftershock dataset, achieved better event detection and phase picking accuracy than conventional methods, while Wang et al.'s (2019) PickNet algorithm has struck a new balance between computational efficiency and localization accuracy. The primary strength of deep learning lies in its ability to autonomously extract features from vast labeled datasets, allowing neural networks to capture the intrinsic characteristics of seismic waveforms without relying on manually preset parameters. Taking PhaseNet as an example, after being trained on a multiphase dataset spanning nearly 90 years from the Northern California seismic

network, it has demonstrated outstanding generalization performance even in regions with significantly different tectonic environments (Zhao, 2021; Su, 2021).

This study employs the deep learning algorithm PhaseNet to systematically analyze the earthquake sequence in the Hefei region of Anhui Province from September 18 to 19, 2024. Using continuous waveform data from the Anhui seismic network, the algorithm is validated against observational data collected during the active aftershock period following the mainshock. The automated detection results are compared multidimensionally with traditional manually processed catalogs, with a focus on evaluating improvements in microearthquake detection accuracy, event detection completeness, and hypocenter localization precision. Experimental results demonstrate that this technique significantly enhances regional seismic monitoring efficiency, particularly in the detailed characterization of earthquake clusters. To further analyze the seismic activity in this region, the research team retrospectively processed continuous waveform data from February 24 to December 21, 2024, constructing a high-resolution earthquake catalog. By integrating high-precision earthquake relocation with an analysis of the regional tectonic framework, they revealed the spatiotemporal migration patterns of seismicity and identified the seismogenic structures.

2. Data and methods

2.1. Tectonic background

The epicentral area is located in the southern segment of the Tanlu Fault Zone (TLFZ), one of the most active deep fault systems in eastern China. This fault zone trends generally north-northeast, extending from the Yilan–Yitong and Dunhua–Mishan faults in the north to Wuxue in Hubei Province in the south, traversing various tectonic units including the Yangtze Block, the Dabie–Sulu orogenic belt, the North China Craton, and the eastern part of the Central Asian Orogenic Belt (the Xingmeng orogenic belt), with a total length of approximately 2400 km (Zhu, 2016), as shown in Fig. 1a. Seismicity along the Tanlu Fault Zone exhibits distinct segmentation; for instance, the 8.5-magnitude earthquake in Tancheng, Shandong, in 1668 and the 7.4-magnitude event in Bohai in 1969 both occurred in the central segment. The Tancheng earthquake remains the largest recorded event in eastern China's history, causing over 50,000 fatalities. Notably, although strong earthquakes of magnitude 6 or above are rarely observed in the southern segment, its position as the structural boundary between the North China Craton and the South China Block (Li, 2023) and its complex tectonic background make it a focal point for research. The southern segment of the Tanlu Fault Zone extends in a northeast to north-northeast direction, characterized by a shallow, branched, and floral fault structure (Li, 2023). It is mainly composed of four nearly parallel faults arranged from west to east: the Wuhe–Hefei fault, the Zhuding–Shimenshan fault, the Chihe–Taihu fault, and the Jiashan–Liujiang fault; the Feizhong fault is located to the north, and

the Chaohu fault to the south. The Zhuding–Shimenshan Fault is west-dipping, while the Chihe–Taihu Fault forms the eastern boundary of the Hefei Basin. The latter exhibits very conspicuous remote sensing features and represents a composite expression of a deep-seated concealed strike-slip fault combined with a shallow extensional fault. Upon entering the Hefei Basin, it continues to extend southward, delineating the boundary between the middle–Neogene strata of the basin and the Zhangbaling Uplift/Feidong Group. The two faults have opposite trends, resulting in the formation of a secondary depression—the Feidong Depression—within the Hefei Basin (Zhao, 2019; Zhang, 2010). The Feidong earthquake occurred at the junction of the Chihe–Taihu fault and the Feizhong fault, as shown in Fig. 1b. Historical seismic records indicate that within a 100 km radius of the epicenter, there were the 1673 Hefei earthquake (M5 at 34 km), the 1868 Dingyuan earthquake (49 km), and the 1585 secondary earthquake in Chaoxian (87 km). It is noteworthy that the Feidong earthquake sequence exhibited high-frequency activity; records from the Anhui seismic network show that a total of 404 events were recorded between February 24 and December 21. This event not only disrupted the long-term low-magnitude activity observed in the southern segment of the Tanlu Fault Zone but also provided an important case study for understanding the nucleation mechanism of moderate-to-large earthquakes in plate-edge tectonic belts.

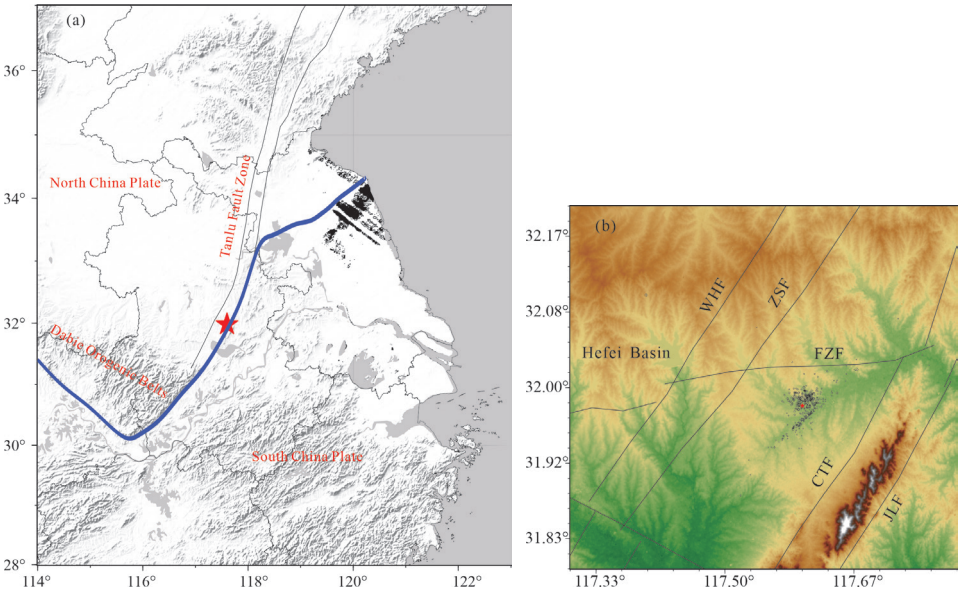

Figure 1. (*a*) Simplified geological map; (*b*) Manual earthquake catalog and tectonic structures in the seismogenic zone. The red pentagon denotes the mainshock, the black circles represent the Feidong sequence earthquakes, and the black lines indicate faults: the Feizhong Fault (FZF), the Wuhe-Hefei Fault (WHF), the Zhuding-Shimenshan Fault (ZSF), the Chihe-Taihu Fault (CTF), and the Jiashan-Liujiang Fault (JLF).

2.2. Data

According to the Anhui seismic network catalog, a total of 404 earthquakes with $M_L \geq 0.0$ were recorded from February 24 to December 21, comprising 30 events in the M_L 0.0–0.9 range, 285 events in the M_L 1.0–1.9 range, 74 events in the M_L 2.0–2.9 range, 10 significant events in the M_L 3.0–3.9 range, 4 strong events in the M_L 4.0–4.9 range, and 1 event with $M_L \geq 5.0$. The largest aftershock in the sequence occurred on September 25 at 19:29, registering an M_L of 4.3 (*Ms* 3.8). As shown in Fig. 2, the temporal evolution of the sequence exhibits distinct phases. Following the *Ms* 3.5 event on February 24, the region experienced 8 minor events, followed by a 22-day quiescent period before the *Ms* 3.1 event on May 12. Up to August 20, intermittent minor seismicity resumed, with the longest quiet period lasting approximately 15 days, followed by a subsequent 20-day calm period. From September 9 onward, minor earthquake activity increased significantly, with a *Ms* 3.9 foreshock occurring on September 14, followed by 3 relatively calm days. On September 18, the region entered an active phase, culminating at 20:08 with the *Ms* 4.7 mainshock. The aftershock sequence following the mainshock decayed rapidly, with 3 aftershocks of $Ms \geq 3.0$ recorded in total, including the *Ms* 3.8 event on September 25 and the *Ms* 3.3 event on October 1. The largest aftershock reached *Ms* 2.6, resulting in a magnitude difference of $\Delta M = 2.1$ between the mainshock and the largest aftershock—characteristic of a typical foreshock–mainshock–aftershock decay pattern.

2.3. Phase picking

PhaseNet relies on only one external parameter—the probability threshold for picking. Its architecture, based on U-Net, takes a 30-second waveform from three components (*Z*, *N*, *E*) as input and outputs three channels corresponding to the probability values for P-wave, S-wave, and noise, respectively, with values ranging from 0 to 1. A probability value closer to 0 indicates a higher likelihood

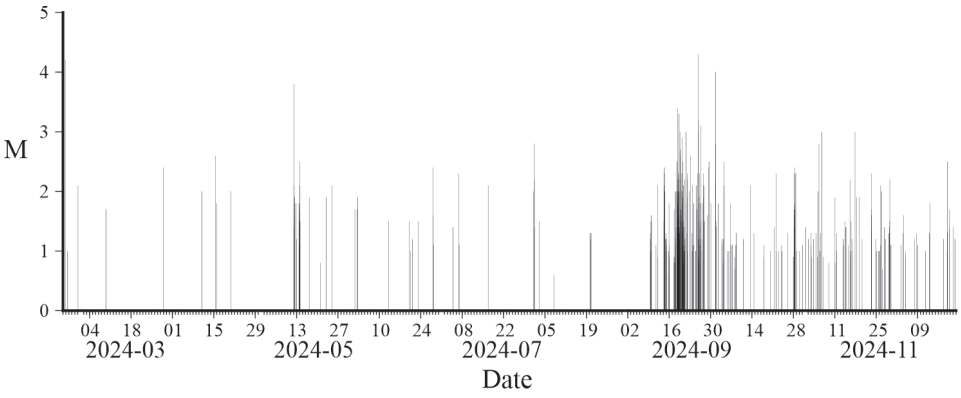

Figure 2. Daily frequency chart of the Feidong earthquake sequence.

that the data point is noise, whereas a value closer to 1 suggests it is more likely an earthquake signal (Zhu, 2019). In deep learning, evaluation metrics such as precision, recall, and the F1 score are commonly used to assess performance. The F1 score is particularly useful for identifying an optimal threshold that balances precision and recall. However, because manual phase picking often fails to capture all genuine seismic phases, precision may be underestimated, thus impeding the accurate determination of the probability threshold solely via the F1 score. Therefore, this study integrates a correlation algorithm to optimize threshold selection, thereby improving the model's accuracy and reliability.

2.4. Association and relocation

Event association is fundamental to earthquake location, and accurate phase association can effectively eliminate misidentified phases. In this study, we adopt the Group Trigger Method used by the Japan Meteorological Agency. The core idea of this method is to identify earthquake events through coordinated triggers from multiple seismic stations. Seismic signals are identified by comparing amplitudes, and when a sufficient number of stations are triggered within a specified time window, the system deems that an earthquake event has been detected. The initial P-wave arrival times obtained from these triggered stations are then used to perform a preliminary earthquake relocation, a process referred to as the "first round of relocation." Subsequently, the initial location is refined by reselecting the P- and S-wave arrival times, followed by a "second round of relocation." This iterative process continues until the earthquake location converges to a relatively stable position (Tamaribuchi, 2018). Building on the phase association and preliminary relocation, the NLLoc program is then employed to further optimize the location results.

In conjunction with the two mobile stations deployed by the Anhui network at the epicenter, this study employs stringent association criteria during event association, requiring a minimum of four seismic phases for relocation; otherwise, the event is discarded. In seismic magnitude calculation, we first use simulation algorithms to simulate velocity waveforms, stripped of instrument response, into DD - 1 displacement records. Then, we measure the maximum amplitude near S or Lg waves. Finally, following the definition in "Seismic Magnitude Regulations" (DB17740 - 2017), we calculate the local magnitude M_L using the formula below.

$$M_L = \lg\left(\frac{A_N + A_E}{2}\right) + R(\Delta)$$

In the formula, A_N and A_E are the maximum amplitudes of S or Lg waves on the NS and WE components, in units of μm. Δ is the epicentral distance in km. $R(\Delta)$ is the calibration function for local magnitude.

2.5. Analysis of testing results

The earthquake localization process in Hefei involves real-time transmission of continuous waveform recordings to the Anhui Seismic Network, where analysts manually pick phase arrivals. Automated algorithms then determine earthquake locations and magnitudes, ultimately generating phase reports. To determine the optimal probability threshold for this region, we applied PhaseNet to process continuous waveform data from September 18 to 19, 2024 (a total of two days). We tested different probability thresholds for phase picking and compared the results with the manually compiled earthquake catalog. The manual catalog identified 87 seismic events. As shown in Table 1, thresholds below 0.3 successfully detected all manually identified events. However, when using thresholds of 0.4 and 0.5, some events were missed, primarily due to high background noise, which prevented PhaseNet from identifying a sufficient number of phases for association. Lin (2022) demonstrated in the Ridgecrest and Weiyuan earthquake sequences that PhaseNet's performance is highly dependent on threshold selection. When the threshold was set to 0.8, the precision rates for P- and S-wave detection reached 96.3% and 97.0%, respectively. Additionally, at lower thresholds (≤0.5), the recall rate for both P- and S-waves remained around 90%. Lin (2022) further evaluated PhaseNet's accuracy, reporting F1 scores ranging from 85% to 91%, with optimal thresholds of 0.35 for P-waves and 0.3 for S-waves. Zhu (2023) constructed regional seismic phase picking models across various regions of China using the PhaseNet architecture combined with the Diting dataset, with both P- and S-phase probability thresholds set to 0.3, yielding favorable detection results.

Considering the test results of this study, the optimal probability threshold is set to 0.3. At this threshold, the origin time deviation ranges from –1 to 2 seconds, the location deviation is within 6 km, and the mean deviation of the local magnitude is 0.15, with a maximum deviation of 0.7. A comparative analysis of the detected seismic phases indicates that these deviations primarily stem from the inclusion of distant stations. Manual phase picking typically excludes low signal-to-noise ratio phases from distant stations, whereas PhaseNet incorporates these phases, leading to an overestimation of magnitude. Therefore, with a threshold of 0.3 and a minimum of four associated phases, earthquakes can be accurately detected.

Table 1. Comparison of earthquake event detection and matching rates by phasenet at different thresholds.

Threshold	0.1	0.2	0.3	0.4	0.5	0.6	0.7	0.8	0.9	1
PhaseNet	2908	381	215	166	105	73	54	37	18	14
Match ratio (%)	100	100	100	91.9	82.8	67.8	55.2	35.6	14.9	11.5

3. Seismic activity characteristics

3.1. Location results

A comprehensive earthquake catalog serves as the foundation for studying seismic activity characteristics and seismogenic structures. Based on the PhaseNet test results, a threshold of 0.3 and a minimum of four associated phases were selected to retrospectively process the continuous waveform data of the Feidong earthquake sequence from February 24, 2024, to December 21, 2024. Through the complete processing workflow, a total of 588 earthquake events were detected—approximately 1.5 times the number identified in the manually processed catalog—resulting in a more complete seismic catalog for analyzing the current seismic activity in Feidong. The relocation results (Fig. 3) show that the spatial distribution of earthquake events exhibits significant clustering, primarily bounded by the Zhuding–Shimenshan Fault, the Chihe–Taihu Fault, and the Feizhong Fault. The overall dominant orientation is toward the NE, and the focal depths are mainly between 7 and 13 km.

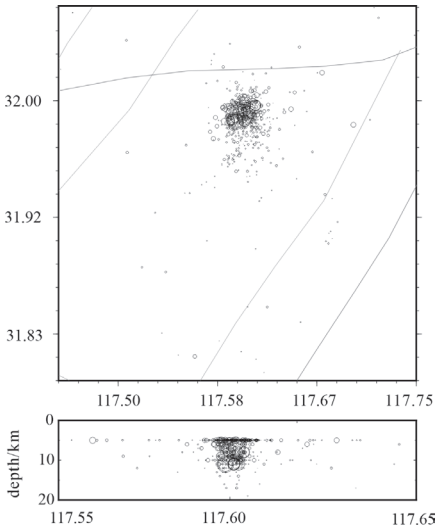

Figure 3. Epicenter distribution of the earthquake catalog.

3.2. High-precision relocation results

To further improve the accuracy of earthquake location determination, this study employs the relative relocation algorithm HypoDD for earthquake relocation. This algorithm determines earthquake locations by analyzing the residual travel-time differences between two seismic events recorded at the same station. According to the study by Waldhauser et al. (2000), when the distance between

two earthquake events is significantly smaller than their distances to the seismic station, their propagation paths to the station can be considered nearly identical. As a result, the observed travel-time differences primarily reflect the spatial differences between the events themselves. As a relative relocation method, the double-difference (DD) location technique effectively reduces the impact of velocity structure variations on earthquake location accuracy. This method is well-established and has been widely applied in earthquake relocation studies, including major earthquakes such as the Wenchuan, Yushu, Lushan, and Jiuzhaigou earthquakes (Chen Jiuhui et al., 2009; Fang Lihua et al., 2011; Yi Guixi et al., 2017).

The spatial distribution characteristics of an earthquake sequence are key constraints in revealing the fault geometry and rupture process. The Feidong M4.7 earthquake sequence exhibited abundant aftershocks. By applying the HypoDD algorithm, we relocated 588 detected earthquakes with high precision, obtaining the epicenter and focal depth distribution for both the mainshock and aftershocks. The results indicate that the precisely relocated coordinates of the mainshock are 32.98°N, 117.60°E, with a focal depth of 11.16 km. Compared to the PhaseNet results (Fig. 3), the relocated earthquakes show a more concentrated distribution, with a clearer linear pattern. The earthquake sequence overall aligns in a NE–SW direction, extending approximately 12 km, nearly parallel to the regional fault of the Tanlu Fault Zone. The cross-sectional profile along the AA' transect (NE-SW direction, 13 km in length, Fig. 4b shows that aftershock focal depths are primarily concentrated between 8–13 km, with only a few events reaching depths of 20 km. After relocation, the focal depths are more clustered, forming a nearly vertical seismic belt, suggesting a steeply dipping fault plane. Observing the depth variations along the AA' transect, most aftershocks exhibit minor depth fluctuations around the mainshock, indicating that

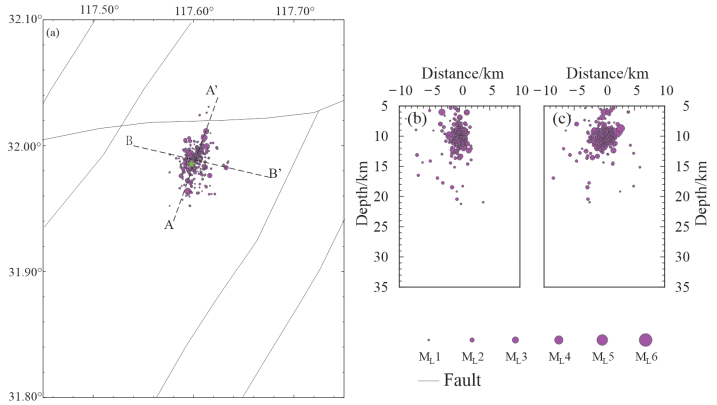

Figure 4. Spatial distribution of the Feidong M4.7 earthquake sequence after double-difference relocation. (*a*) Epicenter distribution after precise relocation. (*b*) Cross-sectional profile along transect AA'. (*c*) Cross-sectional profile along transect BB'.

the rupture primarily occurred at a consistent depth along the NE–SW direction, with the estimated seismogenic fault depth ranging from 8 to 13 km. Furthermore, the BB' transect (NW–SE direction, 18 km in length, Fig. 4c reveals that the mainshock and the majority of aftershocks are concentrated within a compact

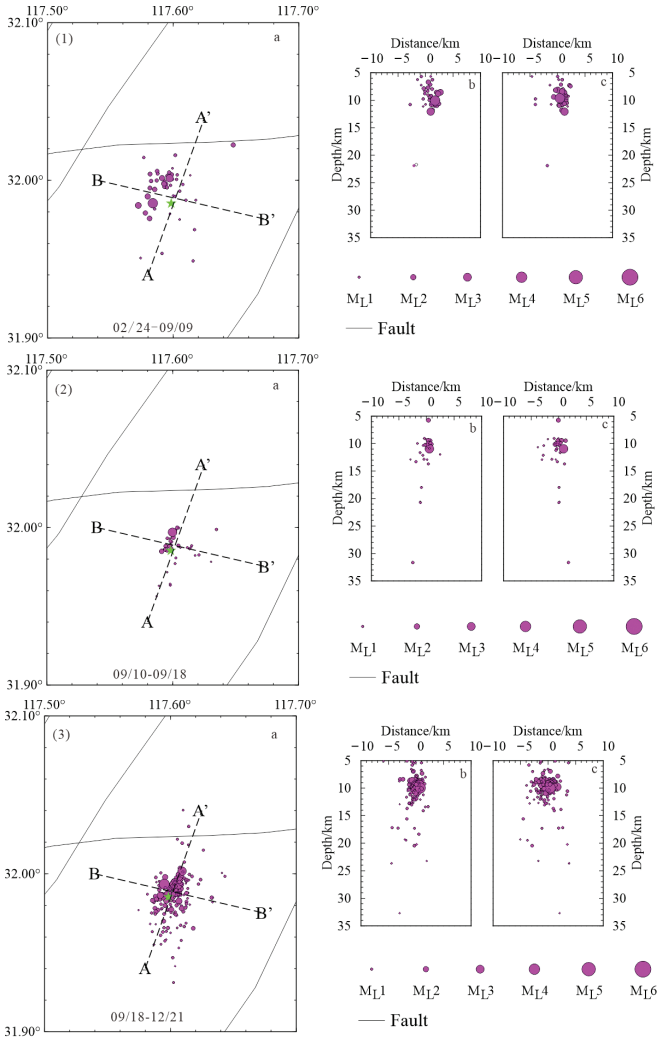

Figure 5. The spatial distribution of the Feidong earthquake sequence during different time intervals. Panel (1) shows seismic activity from February 24 to September 9, 2024; panel (2) represents the period from September 10 to the occurrence of the mainshock (M4.7) on September 18; and panel (3) presents the aftershock distribution from September 18 to December 21. In each subfigure, (*a*) displays the epicenter distribution after high-precision relocation; (*b*) and (*c*) present cross-sectional views of hypocenter distribution along the AA′ and BB′ profiles, respectively, illustrating the vertical migration patterns of seismicity.

region near the mainshock epicenter. This block-like distribution suggests that the seismogenic fault plane is nearly vertical.

To further analyze aftershock migration and the rupture characteristics of the seismogenic fault, the Feidong earthquake sequence data were divided into three time periods for comparative analysis, based on the marked phase characteristics of seismic activity (Fig. 5). The sequence commenced with a significant *Ms* 3.5 event on February 24, followed by a six-month period of intermittent activity. During this initial phase, seismicity was dominated by low-intensity, minor earthquakes ($M_L \leq 2.9$) with a spatial distribution exhibiting a dominant NE trend, and the early clusters were concentrated to the northwest of the mainshock epicenter (approximately at an azimuth of 300°). Starting from September 9, both the frequency of seismic events and the released energy increased markedly, indicating that the fault zone had entered a pre-instability stage. On September 14, an *Ms* 3.9 foreshock occurred, and subsequent aftershock clusters gradually migrated toward the southeast of the mainshock epicenter (the *Ms* 4.7 event on September 18), forming the early stages of a NE-trending linear distribution. Analysis along the AA' transect reveals that during this period, the focal depths exhibited a trend of increasing depth from approximately 5 km at shallow levels to about 10 km at greater depths, suggesting a downward dip along the NE strike within the fault zone. Following the mainshock, the aftershock sequence quickly migrated along the NE–SW direction, with the spatial distribution expanding approximately 6 km on both sides of the mainshock epicenter and forming a NE-trending rupture zone (strike ~45°). The BB' transect further shows that the aftershocks are primarily distributed within a depth range of 5–15 km beneath the mainshock, and that early aftershocks display a migration from shallower to intermediate depths.

3.3. Focal mechanism solution and fault rupture mechanism

In the previous section, the precise relocation of aftershocks provided an initial determination of the causative fault for the Feidong earthquake. To gain a more accurate understanding of the rupture and kinematic characteristics of this earthquake and to better explore the relationship between seismic activity and geological structures, this study employs the widely used Cut and Paste (CAP) method to invert the focal mechanism solution and determine the optimal centroid depth of the earthquake. The CAP method calculates the focal mechanism solution through waveform fitting, assigning different weights to body waves and surface waves. It then determines the cross-correlation coefficients and misfit functions between the observed and theoretical waveforms for body and surface waves (Fu et al., 2019). A grid search is performed to identify the fault plane parameters (double-couple nodal plane parameters) and the optimal centroid depth that yield the highest similarity between theoretical and observed waveforms. Since the CAP method jointly inverts body and surface waves, it reduces dependence on the crustal velocity structure and provides an accurate

centroid depth (Luo et al., 2015). This makes it suitable for analyzing seismogenic structures and earthquake-generating environments. In recent years, it has been widely applied (Zheng et al., 2009).

In selecting the stations for this study, only those within 300 km with good coverage were chosen. The precise locations and event times obtained through double-difference positioning served as reference data for the CAP method in source mechanism inversion. During the inversion process, waveforms from 0 to 300 seconds were extracted and subjected to zero drift and mean removal. Consistency among header file values was checked and corrected when discrepancies were found. For body waves, a time window of 35 seconds was selected with a band-pass filter range of 0.05–0.18 Hz; for surface waves, a 75-second time window with a 0.05–0.08 Hz band-pass filter was used. Based on existing research, weights of 2 and 1 were assigned to body and surface waves, respectively, to balance their contributions (Zhu and Helmberger, 1996; Kang et al., 2025). Theoretical seismograms were calculated using the frequency-wavenumber (F-K) method with the same band-pass filter as the observed waveforms (Tan et al., 2006). Waveform fitting was performed between observed and theoretical seismograms. The source mechanism solution with the minimum global fitting residual was identified as the optimal source mechanism for this earthquake.

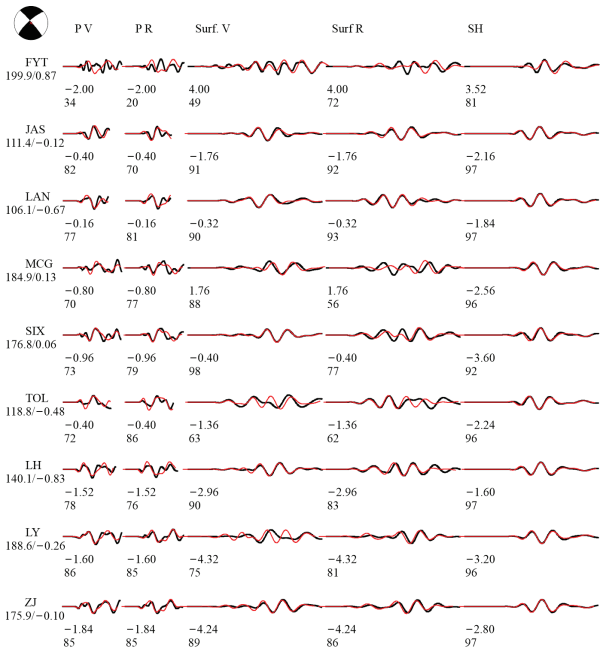

Figure 6. The optimal source mechanism solution and its theoretical waveform are compared with the actual waveform.

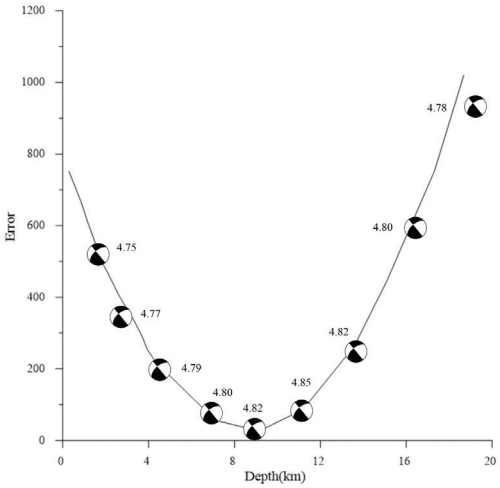

Figure 7. The fitted residuals and the source mechanism solutions change with depth.

Figure 6 illustrates the fitting between observed and theoretical waveforms from various stations during the source mechanism inversion process. The data from nine participating stations encompass 45 seismic phases. The observed waveforms align well with the theoretical ones, with most correlation coefficients exceeding 70%, indicating that the theoretical waveforms effectively replicate the observed data, thereby enhancing the reliability of the source mechanism inversion results.

Figure 7 presents source mechanism solutions and waveform fitting residuals at different source depths. The inversion results for the two fault plane parameters remain relatively stable across varying depths. The residuals between observed and theoretical waveforms reach a minimum when the source depth is 10.3 km, suggesting that this depth corresponds to the optimal source depth for the earthquake. This optimal depth aligns closely with the source depth calculated using the double-difference location method, further corroborating the reliability of the inverted source mechanism solution.

Table 2. Focal mechanism solutions for $M \geq 3$ earthquakes in the Feidong.

Event date	M	Plane I			Plane II		
mm-dd		Strike	Dip	Rake	Strike	Dip	Rake
02-24	3.7	41	82	–174	310	84	-8
05-12	3.2	226	70	171	319	82	20
09-14	3.9	227	79	171	319	81	11
09-18	4.7	228	77	176	319	86	13
09-25	3.8	226	89	172	316	82	1
10-01	3.4	236	65	171	330	82	25

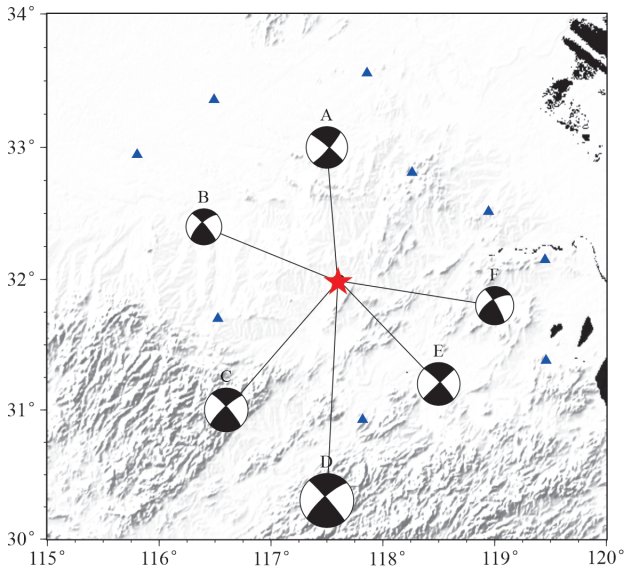

Figure 8. Focal mechanism solutions for M≥3 earthquakes in the Feidong seismic source region and station location map.

The optimal source mechanism solution is characterized by: fault plane I having a strike of 227°, dip of 79°, and rake of –171°; fault plane II with a strike of 319°, dip of 86°, and rake of 13°; and a moment magnitude of M_W 4.82. Table 2 and Fig. 8 summarizes the source mechanism solutions for all six earthquakes of magnitude 3 and above in the Feidong region during 2024, highlighting their consistency. These findings confirm that the Feidong M4.7 earthquake sequence is primarily strike-slip in nature, aligning with the regional NEE-SSW compressive stress field (Ni et al., 2021).

4. Discussion

4.1. Seismogenic structures and regional tectonic background of the Feidong earthquake sequence

The Feidong M4.7 earthquake exhibits distinct phased characteristics in terms of its temporal evolution. Since February 2024, seismic activity in the region has gradually intensified, with a notable increase in both frequency and magnitude of earthquakes after September 10. This temporal evolution is likely related to the gradual accumulation and release of regional stress. In terms of spatial distribution, the earthquake sequence is primarily aligned in a NE–SW direction, with a length of approximately 12 km, and focal depths are concentrated between 8 and 13 km. This spatial distribution suggests that the seismogenic fault in the region has a certain degree of extension and depth range. The aftershock sequence

exhibits a linear NE alignment, with a total extension length of about 12 km and focal depths concentrated at approximately 10.5 km. This aligns well with the orientation and structural characteristics of the major regional fault—the Zhuding-Shimenshan Fault. Focal mechanism inversion results further indicate that all six major earthquakes in the region exhibit right-lateral strike-slip characteristics on a high-angle fault dipping to the NE (Fig. 8). This result is consistent with measurements of the regional tectonic stress field (Liu, 2015). These observations suggest that the seismogenic structure of the Feidong earthquake is likely a single fault, with a strike and dip angle that conform to the characteristics of a right-lateral strike-slip fault. It is inferred that this fault may represent an active segment of the Zhuding-Shimenshan Fault.

4.2. Seismic environment analysis

According to Li (2023), using full-waveform inversion methods, the region between the Chihe-Taihu Fault and the Jiashan-Lujiang Fault is located in a high-velocity zone. The surface lithology indicates that magma beneath the surface may have intruded during the shear strike-slip extension process of the Tanlu Fault. The Feidong earthquake sequence is concentrated at the boundary between high and low-velocity zones, and this velocity contrast may lead to stress concentration and accumulation, providing favorable conditions for the occurrence of earthquakes. Aftershock relocations show that the mainshock and most aftershocks are concentrated at depths of 8–13 km (Fig. 4b), which coincides with the upper part of the crustal brittle-ductile transition zone in the region (Li, 2023). The Zhuding–Shimenshan Fault gradually extends eastward at depth and intersects the Chihe–Taihu Fault in the deeper crust. Coupling this with evidence of fluid intrusion, it is inferred that fluids may have migrated into the seismogenic zone from the southwest via structural conduits such as the Zhuding–Shimenshan Fault. Within a depth range of 0–15 km near the fault, the accumulation of fluids could induce stress changes on the fault plane, thereby promoting slippage and instability (Zhang et al., 2023; Kim et al., 2023).

5. Conclusion

The 4.7 magnitude earthquake that occurred on September 18, 2024, in Feidong County, Hefei City, Anhui Province, is the largest earthquake in modern history in the Hefei region, causing significant social impact. This study employs deep learning to identify the Feidong earthquake sequence and conducts precise location analysis on the detected sequences. By combining source mechanism inversion and a comprehensive analysis of the seismogenic environment, the following main conclusions are drawn:

The spatiotemporal distribution of the Feidong earthquake sequence exhibits pronounced tectonic control. The sequence is linearly distributed along a

NE–SW trend, and focal mechanism inversions for the six major events indicate that they all display high-angle right-lateral strike-slip characteristics with a NE trend and a consistent dip direction. Combined with the regional tectonic features, this suggests that the seismogenic fault associated with the Feidong earthquake belongs to the active segment of the Zhuding–Shimenshan Fault. Furthermore, incorporating evidence of fluid intrusion, it is inferred that fluids may enter the seismogenic zone from the southeast through structural conduits such as the Zhuding–Shimenshan Fault and accumulate within a depth range of approximately 10 km near the fault. This fluid buildup likely leads to localized stress concentration, which may have triggered the Feidong earthquake sequence.

Acknowledgments – We sincerely acknowledge the support from the Monitoring and Early Warning Task of China Earthquake Administration (Project No.: CEA-JCYJ-202501040).

References

Chen, J. H., Liu, Q. Y., Li, S. C., Guo, B., Li, Y., Wang, J. and Qi, S. H. (2009): Relocation of the Wenchuan M_S8.0 earthquake aftershock sequence and its seismotectonic implications, *Chinese J. Geophys.*, **52**(2), 390–397 (in Chinese).

Fang, L. H., Wu, J. P., Zhang, T. Z., Huang, J., Wang, C. Z. and Yang, T. (2011): Relocation of the 2011 Yingjiang, Yunnan M_S5.8 earthquake and its aftershock sequence, *Acta Seismol. Sin.*, **33**(2), 127–135, https://doi.org/10.3969/j.issn.0253-3782.2011.02.013.

Fu, H., Jiang, J. Z., Li, J. and Pan R. (2019): Focal mechanism solutions and depth determination of the 2017 Yangbi, Yunnan M_S5.1 and M_S4.8 earthquakes, *J. Seismol. Res.*, **42**(3), 338–348, https://doi.org/10.3969/j.issn.1000-0666.2019.03.005.

Kim, D., Jung, H. and Lee, J. (2023): Impact of chlorite dehydration on intermediate-depth earthquakes in subducting slabs, *Communications Earth & Environment*, **4**, 491, https://doi.org/10.1038/s43247-023-01133-5.

Kang, Q., Yu, Y., Gu, O., Li, L. L., Liu, F., Wang, W., Yang, Y., Wang, J. F., Xu, T., Zhou, Y. C., Sun, X. H. and Sun, Z. Q. (2025): Focal mechanism solutions and seismogenic structure of the M 5.0 earthquake in the sea area near Dafeng, Jiangsu Province on November 17, 2021, *Chinese J. Geophys.*, **68**(5), 1884–1895, https://doi.org/10.6038/cjg2024R0640 (in Chinese).

Li, H., Li, J., Luo, S., Bem, T. S., Yao, H. and Huang, X. (2023): Continent-continent collision between the South and North China plates revealed by seismic refraction, *Geophys. Res.: Solid Earth*, **128**(1), e2022JB025748, https://doi.org/10.1029/2022JB025748.

Lin, X. K. and Xu, C. J. (2022): Deep learning-driven seismic catalog construction: Comparison and evaluation of PhaseNet and EqT models, *Geomatics and Information Science of Wuhan University*, **47**(6), 903–912, https://doi.org/10.13203/j.whugis20220197.

Liu, B., Zhu, G., Zhai, M. J., Gu, C. C., Song, L. H. and Liu, S. (2015): Characteristics and genesis of active faults in the Anhui segment of the Tanlu Fault Zone, *Geological Science*, **50**(2), 611–630, https://doi.org/10.3969/j.issn.0563-5020.2015.017.

Luo, Y., Zhao, L., Zeng, X. and Guo Y. (2015): Focal mechanisms of the Lushan earthquake sequence and spatial variation of the stress field, *Sci. China Earth Sci.*, **58**, 1148–1158, https://doi.org/10.1007/s11430-014-5017-y.

Ni, H. Y., Tan, Y. P., Deng, L., Wang, X. L., Bao, Z. W., Fang, Z. and Hong, D. Q. (2021): Detection of missed earthquakes and seismogenic structure analysis of the 2014 Jinzhai M_L3.9 earthquake swarm, *Seismology and Geology*, **43**(2), 456–468, https://doi.org/10.3969/j.issn.1001-4683.2021.02.011.

Shelly, D. R., Beroza, G. C. and Ide, S. (2007): Non-volcanic tremor and low-frequency earthquake swarms, *Nature*, **446**, 305–307, https://doi.org/10.1038/nature05666.

Su, J. B., Liu, M., Zhang, Y. P., Wang, W. T., Li, H. Y., Yang, J., Li, X. B. and Zhang, M. (2021): High-resolution seismic catalog of the May 21, 2021 Yangbi, Yunnan M_S6.4 earthquake sequence based on deep learning, *Chinese J. Geophys.*, **64**(8), 2647–2656, https://doi.org/10.6038/cjg2021O0530.

Tamaribuchi, K. (2018): Evaluation of automatic hypocenter determination in the JMA unified catalog, *Earth Planets Space*, **70**, 141, https://doi.org/10.1186/s40623-018-0915-4.

Tan, Y., Zhu, L., Helmberger, D. V. and Saikia, C. K. (2006): Locating and modeling regional earthquakes with two stations, *J. Geophys. Res.-Atmos.*, **111**(B1), https://doi.org/10.1029/2005JB003775.

Waldhauser, F. and Ellsworth, W. L. (2000): A double-difference earthquake location algorithm: Method and application to the northern Hayward fault, California, *Bull. Seismol. Soc. Am.*, **90**(6), 1353–1368, https://doi.org/10.1785/0120000006.

Wang, J., Xiao, Z., Liu, C., Zhao, D. and Yao, Z. (2019): Deep learning for picking seismic arrival times, *J. Geophys. Res.: Solid Earth*, **124**(7), 6612–6624, https://doi.org/10.1029/2019JB017536.

Yuan, A. J. (2022). Microseismic scanning and seismic activity study in the North Tianshan seismic belt. Master's thesis, Institute of Earthquake Forecasting, China Earthquake Administration. https://doi.org/10.27488/d.cnki.ggjfz.2022.000015.

Yi, G. X., Long, F., Liang, M. J., Gong, Y., Qiao, H. Z., Wang, Z., Qiu, G. L., Su, J. R., Zhang, H. P. and Zhao, M. (2017): Focal mechanism solutions and seismogenic structure analysis of the August 8, 2017 Jiuzhaigou M7.0 earthquake and its aftershocks, *Chinese J. Geophys.*, **60**(10), 4083–4097.

Zhang, J. D., Yang, C. C., Liu, C. Z., Liu, D. L., Yang, X. Y., Liu, C. F., Huang, S. and Lin, F. L. (2010): The deep structures of strike-slip and extension faults and their composite relationship in the southern segment of Tanlu Fault Zone, *Chinese J. Geophys.*, **53**(4), 864–873, https://doi.org/10.3969/j.issn.0001-5733.2010.04.011.

Zhang, M., Ellsworth, W. L. and Beroza, G. C. (2019): Rapid earthquake association and location, *Seismol. Res. Lett.*, **90**(6), 2276–2284, https://doi.org/10.1785/0220190052.

Zhang, Y. P., Wang, W. T., Yang, W. and Liu Y. (2023). Inversion of 3D crustal velocity structure in the southern segment of the Tanlu Fault Zone by joint multi-source data, *Chinese J. Geophys.*, **66**(6), 2404–2419, https://doi.org/10.6038/cjg2022Q0336.

Zhao, M., Tang, L., Chen, S., Su, J. B. and Zhang, M. (2021): Automatic construction of the foreshock catalog of the Changning earthquake based on deep learning arrival-time picking, *Chinese J. Geophys.*, **64**(1), 13–26, https://doi.org/10.6038/cjg2021O0271.

Zhao, W. D., Zheng, Y., Zhang, H. N., Jiang, Q. and Wei, J. J. (2019): Remote sensing interpretation and spatial distribution characteristics of the Anhui segment of the Tanlu Fault Zone based on multi-source data, *Remote Sensing for Land and Resources*, **31**(4), 99–107, https://doi.org/10.6046/gtzyyg.2019.04.11.

Zheng, Y., Ma, H. S., Lü, J., Ni, S. D., Li, Y. C. and Wei, S. J. (2009): Focal mechanisms of strong aftershocks (M_S≥5.6) of the Wenchuan earthquake and their relationship to seismogenic structures., *Sci. China Earth Sci.*, **39**(4), 413–426.

Zhou, B. W. (2021): Automatic seismic detection method and application based on convolutional neural networks. Master's Thesis, Institute of Geophysics, China Earthquake Administration, https://doi.org/10.27487/d.cnki.gzdws.2020.000019.

Zhou, Y., Yue, H., Kong, Q. and Zhou, S. (2019): Hybrid event detection and phase-picking algorithm using convolutional and recurrent neural networks, *Seismol. Res. Lett.*, **90**(3), 1079–1087, https://doi.org/10.1785/0220180319.

Zhu, G., Wang, W., Gu, C. C., Zhang, S. and Liu, C. (2016): Late Mesozoic evolution of the Tanlu Fault Zone and its implications for the destruction of the North China Craton, *Acta Petrol. Sin.*, **32**(4), 935–949.

Zhu, J., Li, Z. and Fang, L. (2023): USTC-Picker.s: A unified set of seismic phase pickers Transfer learned for China, *Earthquake Science*, **36**(2), 95–112, https://doi.org/10.1016/j.eqs.2023.03.001.

Zhu, L. and Helmberger, D. V. (1996): Advancement in source estimation techniques using broadband regional seismograms, *B. Seismol. Soc. Am.*, **86**(5), 1634–1641, https://doi.org/10.1785/BSSA0860051634.

Zhu, W. and Beroza, G. C. (2019): PhaseNet: A deep-neural-network-based seismic arrival-time picking method, *Geophys. J. Int.*, **216**(1), 261–273, https://doi.org/10.1093/gji/ggy423.

SAŽETAK

Identifikacija mikropotresa i analiza seizmičnosti sekvence potresa magnitude 4,7 u Feidongu, Anhui

Yu Wang, Shiwen Xie, Pan Guo i Junhao Qu

Dana 18. rujna 2024. godine potres magnitude 4,7 pogodio je okrug Feidong u gradu Hefei, u provinciji Anhui. Smješten na rasjednoj zoni Tanlu, ovaj događaj pokazao je jasan slijed predpotres–glavni potres–naknadni potresi, što je privuklo veliku pozornost javnosti u pogođenom području. Kako bi se istražila aktivnost naknadnih potresa i seizmogena struktura ove sekvence potresa, u ovom se istraživanju primjenjuju metode dubokog učenja na kontinuirane valne zapise sakupljene pomoću seizmičke mreže provincije Anhui s ciljem automatske detekcije potresa. U kombinaciji s preciznim relokacijama potresa, izrađen je sveobuhvatan i visoko precizan seizmički katalog potresa. Rezultati relokacije pokazuju da je sekvenca potresa uglavnom raspoređena duž linearne zone u smjeru sjeveroistok–jugozapad, u duljini od oko 12 kilometara, s hipocentrima koncentriranim na dubinama između 8 i 13 kilometara. I glavni potres i većina naknadnih potresa javljaju na dubini od oko 10,5 kilometara. Rješenja žarišnih mehanizama otkrivaju da dominantni potresi u tom području pokazuju desnoručnu rasjednu aktivnost (strike-slip) na strmim rasjedima u smjeru sjeveroistok–jugozapad, što je u velikoj mjeri u skladu s orijentacijom i strukturnim karakteristikama glavnog rasjeda Zhuding–Shimenshan u tom području. U kombinaciji s opažanjima prodora fluida, pretpostavlja se da su se fluidi kretali iz jugozapadnog smjera u seizmogenu zonu kroz rasjed Zhuding–Shimenshan i akumulirali na dubini od približno 10 kilometara u blizini rasjeda. Ta akumulacija fluida vjerojatno je izazvala lokalni porast smicanja, što je moglo biti glavni okidač za sekvencu potresa u Feidongu.

Ključne riječi: dubinsko učenje, premještanje s dvostrukom razlikom, rješenje žarišnog mehanizma, seizmogeni sklop

Corresponding author's address: Shiwen Xie, Gangxi Road, Ganggou Street, Licheng District, Jinan City, Shandong Province, China; e-mail: sdtwczs2@163.com